

Effects of Sb-doped SnO₂–WO₃ nanocomposite on electrochromic performance



Kue-Ho Kim^a, Bon-Ryul Koo^b, Hyo-Jin Ahn^{a,b,*}

^a Department of Materials Science and Engineering, Seoul National University of Science and Technology, Seoul, 01811, South Korea

^b Program of Materials Science & Engineering, Convergence Institute of Biomedical Engineering and Biomaterials, Seoul National University of Science and Technology, Seoul, 01811, South Korea

ARTICLE INFO

Keywords:

Films
Nanocomposites
Electrical properties
Transition metal oxides
Electrochromic performances

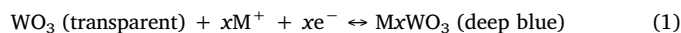
ABSTRACT

With the increase in global challenges related to energy depletion, there is significant emphasis on studies involving next-generation optoelectronic applications such as smart windows and electronic displays. In particular, electrochromic devices (ECDs) have been identified as strategic innovations for energy-saving “smart windows” to address these challenges. Despite this increased level of attentions, ECDs have not yet attained broad commercial acceptance because of their limited electrochromic (EC) properties including coloration efficiency (CE, < 30.0 cm²/C) and switching speeds (> 10.0 s). To address these limitations, critical effort is required to enhance the EC properties by tuning the film structure and electronic structure of ECDs. In this study, we demonstrated the effect of nanocomposite structure of conductive metal oxides and WO₃ EC films. Antimony-doped tin oxide nanoparticles (ATO NPs) were utilized because of their superior electrical conductivity and large band gap. To achieve the optimum addition amount of ATO NPs in EC films, we adjusted the amount as 0, 0.6, 1.2, 2.4 wt%. WO₃ EC films with the optimum addition amount (1.2 wt%) of ATO NPs exhibited improved EC performance including both the switching speeds (5.4 s for the coloration speed and 2.4 s for the bleaching speed) and CE value (48.2 cm²/C). The enhancement of EC performance was attributed to the well-dispersed ATO NPs in the WO₃ films that can effectively improve electrical conductivity via the formation of by forming preferred electron pathway. In addition, the large band gap of ATO NPs broadens the transmittance modulation of the EC layer which contributed to the increment of the CE value. Therefore, our results suggest a strategy to obtain the enhanced WO₃ films with superior EC performances using conductive metal oxides nanocomposite structure.

1. Introduction

The phenomenon called electrochromism is an enabling technology for devices that require variable-optical properties such as digital displays, smart windows, and rear view mirrors [1–3]. Subsequent to the discovery of this phenomenon by Deb et al. [4], electrochromic devices (ECDs) have received significant attention due to their useful characteristics that include color variation, low operating voltage, and transmittance in the visible region [5]. Recently, global challenges related to increasing energy consumption have attracted notable attention in the field of ECDs [6,7]. This has accelerated further research to this field with the objective of improving the electrochromic (EC) properties of these devices. Generally, the ECDs are composed of five functional layers: anodic, cathodic EC layers, ion conductor layer, and the two transparent conducting layers [8,9]. Among them, it is well

known that the EC layers play a predominant role because the key performances of ECDs (transmittance modulation, switching speed, and CE) are determined by the electrochemical reaction that occurs at the EC layers [10,11]. Transition metal oxides are mainly used in the EC layers. In particular, tungsten oxide (WO₃) is one of the most extensively investigated EC materials that is currently used in ECD applications [12–14] due to its superior transmittance modulation and electrochemical stability. WO₃ films can vary their colors from optical transparency to deep blue by small cation (H⁺, Na⁺ and Li⁺) intercalation/deintercalation of their lattice under the application of a voltage bias. This is accompanied by the movement of electrons to an external circuit and the process is described by the following equation (see Eq. (1)) [15]:



* Corresponding authors. Department of Materials Science and Engineering, Seoul National University of Science and Technology, Seoul, 01811, South Korea.
E-mail address: hjahn@seoultech.ac.kr (H.-J. Ahn).

<https://doi.org/10.1016/j.ceramint.2019.05.109>

Received 15 April 2019; Received in revised form 10 May 2019; Accepted 11 May 2019

Available online 12 May 2019

0272-8842/ © 2019 Elsevier Ltd and Techna Group S.r.l. All rights reserved.

However, WO_3 films are still too limited with respect to a low CE value ($< 30.0 \text{ cm}^2/\text{C}$) and slow switching speeds ($> 10.0 \text{ s}$) for EC applications. To address these limitations, it is necessary to facilitate electrochemical reactions that accompanied with ion and electron mobility. The enhancement of the electrical conductivity of EC materials is one of the key factors that directly influence EC performances [16]. It is known that an increase in electrical conductivity can be achieved via doping with metal ions and high conductive composite structures [17–23]. Initially, the doping of metal ions is known to enhance electrical conductivity by providing free charge carriers to the host lattice. Zhou et al. fabricated Ni-doped WO_3 films using the seed-free hydrothermal method. These films exhibited fast switching speeds (6.7 s for the coloration speed and 3.4 s for the bleaching speed) at 0.5 wt% doping concentration [24]. Xie et al. achieved optimized 2 at% Mo-doped WO_3 films using electrodeposition which also exhibited superior switching speeds (2.0 s for bleaching speed and 2.1 s for coloration speed). In addition, a composite structure with a transition metal oxide is also useful for enhancing electrical conductivity via the formation of electron transfer channels that increase electron mobility. Han et al. prepared TiO_2 nanocrystal embedded WO_3 films using a one-step dip-coating method and demonstrated enhanced CE value ($68.1 \text{ cm}^2/\text{C}$) with fast switching speeds (5.0 s for bleaching speed and 3.0 s for coloration speed) due to the reduced Li ion trapping site of the WO_3 structure with embedded TiO_2 nanocrystals [25]. Further, Kim et al. presented results for dual-band electrochromic materials with highly functional electrochemical reactions using a NbO- WO_3 nanocomposite structure [26]. However, despite these efforts, high conductive metal oxide nanocomposite structures for EC material have not been reported to date.

In this regard, we used antimony-doped tin oxide nanoparticles (ATO NPs) to enhance the properties of ECDs and fabricated ATO- WO_3 nanocomposite structure using a low-cost and simple spin-coating method. Well-dispersed ATO NPs in amorphous WO_3 effectively improved EC performances. This improvement was attributed to their unique characteristics that include high electrical conductivity and large band gap. To demonstrate the effect of ATO NPs in WO_3 , we investigated the relationship between their optical, chemical, structural, electrochemical and EC performances.

2. Experimental details

ATO- WO_3 nanocomposite films were fabricated via a spin-coating process using a sol solution with ATO NPs and WCl_6 . Initially, to obtain the ATO NPs using a hydrothermal method, a precursor solution was prepared by dissolving 0.15 M tin chloride pentahydrate ($\text{SnCl}_4 \cdot 5\text{H}_2\text{O}$, SAMCHUN) as a precursor and antimony (III) chloride (SbCl_3 , Aldrich) as a doping agent into de-ionized (DI) water with 4 vol% ammonium hydroxide solution (NH_4OH , Aldrich). In this solution, the molar concentration of the Sb/Sn was fixed as 0.1 M. After stirring for 30 min, the resulting solution was transferred into a Teflon-lined autoclave and hydrothermal reaction occurred at 220°C for 6 h. Afterward, the resultant precipitates were washed with DI water and dried in an oven for 6 h at 80°C , then sintered at 600°C for 3 h to obtain the required crystallinity of the ATO NPs. To prepare the sol solution for the spin-coating process, 10 wt% tungsten (VI) chloride (WCl_6 , Aldrich) was dissolved in 2-propanol ($(\text{CH}_3)_2\text{CHOH}$, Aldrich). After stirring, the ATO NPs were added into the prepared solution. The amount of the ATO NPs added to the solution was set as 0, 0.6, 1.2, and 2.4 wt% to optimize the nanocomposite effect of ATO NPs on the EC performances of the WO_3 films. Then, the sol solutions were spin-coated at 2,000 rpm for 30 s onto commercial fluorine-doped tin oxide (FTO) glass (Pilkington, $8.0 \Omega/\square$). They were then annealed at 300°C in air, resulting in the formation of ATO- WO_3 nanocomposite films with different amounts of ATO NPs that included 0, 0.6, 1.2, and 2.4 wt% (hereafter identified as bare WO_3 , 0.6ATO- WO_3 , 1.2ATO- WO_3 and 2.4ATO- WO_3 , respectively).

The morphology and structure were examined using field-emission

scanning electron microscopy (FESEM, Hitachi S-4800) and transmission electron microscopy (TEM, Gwangju Center, Korea Basic Science Institute). Structural analyses were performed using X-ray diffraction (XRD, Rigaku D/Max – 2500 diffractometer using Cu K α radiation), and the chemical bonding states of the samples were investigated by X-ray photoelectron spectroscopy (XPS, ESCALAB 250 equipped with an Al K α X-ray source). The electrical and optical properties were measured by a Hall-effect measurement system (Ecopia, HMS-3000) and ultraviolet–visible (UV–vis) spectroscopy (Perkim–Elmer, Lambda-35), respectively. The electrochemical and EC performances were characterized using a potentiostat/galvanostat (PGSTAT302 N, FRA32 M, Metrohm Autolab B.V., Netherlands). Measurements were performed using the three-electrode system with 1 M LiClO_4 ($\geq 95.0\%$, Aldrich) in propylene carbonate (anhydrous, 99.7%, Aldrich) as the electrolyte, Pt wire as the counter electrode, and Ag wire as the reference electrode. The diffusion coefficient of all the samples was calculated for various current densities with an increase in the scan rate (20, 40, 60, 80 and 100 mV/s). Ultraviolet–visible (UV–vis) spectroscopy (Perkim–Elmer, Lambda – 35) was performed at 633 nm to analyze the *in situ* optical transmittances which regards the switching speeds of the EC films.

3. Results and discussion

Fig. 1 shows FESEM images of (a) ATO NPs, (b) bare WO_3 , (c) 0.6ATO- WO_3 , (d) 1.2ATO- WO_3 , and (e) 2.4ATO- WO_3 . In the case of the ATO NPs, spherical nanostructures with a diameter in the range of 9.5–13.8 nm were successfully formed using a hydrothermal method. Bare WO_3 samples appear to have a smooth and uniform surface, which implies the formation of amorphous WO_3 (see Fig. 1b). In nanocomposite films, the presence of well-dispersed ATO NPs in the films was clearly observed, which can be explained by the difference in flat-band potential of WO_3 (0.33 V) and SnO_2 (-0.1 V) [25,27]. As such, their opposite charge causes an electrostatic attractive force when they are mixed together, resulting in a homogeneously dispersed colloid [25]. In addition, with an increase in the addition amount of ATO NPs, the distribution of well-dispersed ATO NPs in the films was improved from the 0.6ATO- WO_3 sample (see Fig. 1c) to the 1.2ATO- WO_3 sample (see Fig. 1d), together with a decrease in the distance between the ATO NPs. However, the 2.4ATO- WO_3 sample exhibited an aggregation phenomenon of the ATO NPs with an increase in the distance between the ATO NPs due to the excessive amount of the ATO NPs (see Fig. 1e). Given that the ATO NPs have superior electrical conductivity and a large band gap, their dispersion can enhance the electrical properties of WO_3 films which mainly affects the EC performances. To confirm the quantitative amount of the ATO NPs in the WO_3 films, the ratio of each atoms was investigated using an energy dispersive spectrometer (EDS) and the results are as shown in Table 1. As expected, only W and O atoms were detected in bare WO_3 samples. However, the nanocomposite films exhibited an increased ratio of detected Sn atoms from 0.15 at % for the 0.6ATO- WO_3 samples to 0.68 at% for the 2.4ATO- WO_3 samples. To further investigate the presence of dispersed ATO NPs in the WO_3 films, we performed TEM analyses. Fig. 2 represents the TEM images of the bare WO_3 and 1.2ATO- WO_3 samples. Although a uniform contrast is observed for the bare WO_3 samples (see Fig. 2a), the existence of well-dispersed ATO NPs in the WO_3 films was clearly identified in the 1.2ATO- WO_3 samples (see Fig. 2b). High-resolution TEM images of the 1.2ATO- WO_3 samples (Fig. 2c), demonstrated that the lattice distance of the crystalline NPs is 0.337 nm. This is a higher value than that of pure SnO_2 (0.33 nm), which indicates the formation of the ATO phase [28,29]. In addition, selected area electron diffraction (SAED) pattern of bare WO_3 sample (see insets of Fig. 2a) revealed multiple spread ring that corresponds to an amorphous structure, whereas there are dot patterns related to the crystalline structure of the 1.2ATO- WO_3 samples (see insets of Fig. 2b), together with multiple spread ring pattern. These results prove the successful formation of a nanocomposite film and that crystalline ATO NPs are well-dispersed in

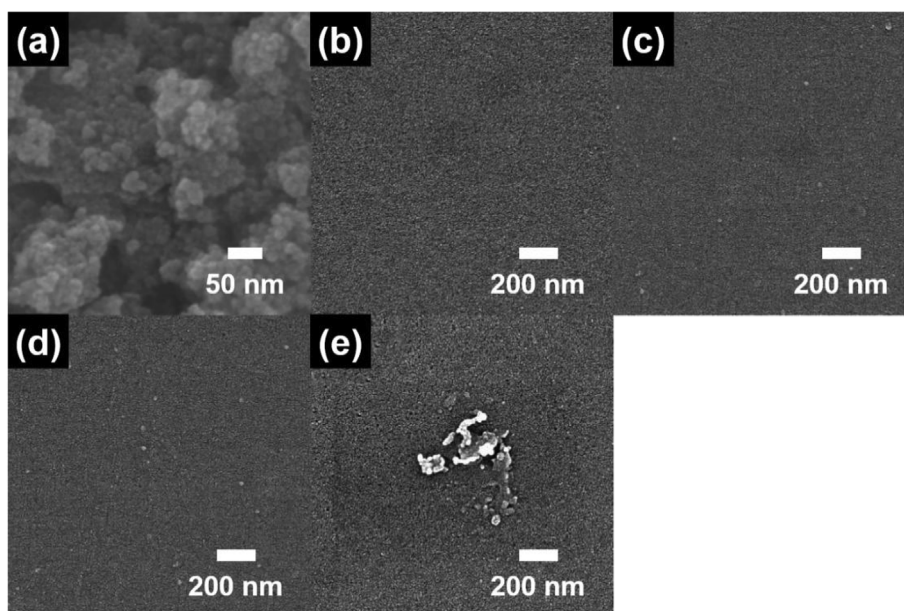


Fig. 1. Top-view FESEM images of (a) ATO NPs, (b) Bare WO_3 , (c) 0.6ATO- WO_3 (d) 1.2ATO- WO_3 and (e) 2.4ATO- WO_3 , respectively.

Table 1
Summary of EDS analysis measured from all samples.

Samples	W (at%)	O (at%)	Sn (at%)
Bare WO_3	11.73	88.27	–
0.6ATO- WO_3	12.64	87.22	0.14
1.2ATO- WO_3	12.03	87.67	0.31
2.4ATO- WO_3	10.47	88.84	0.69

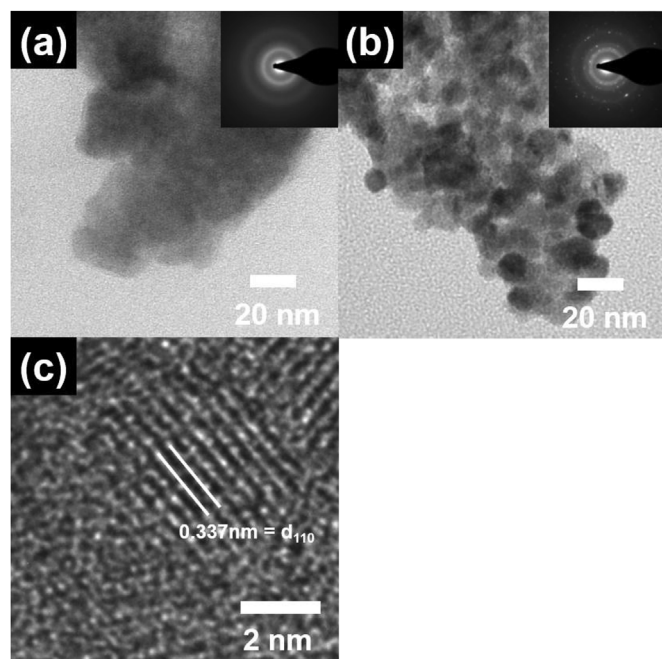


Fig. 2. HRTEM images of (a) Bare WO_3 , (b, c) 1.2ATO- WO_3 , respectively. Their selected area electron diffraction (SAED) patterns are shown in the inset (top right).

the amorphous WO_3 films, which can improve the EC properties due to the high electrical conductivity and large band gap of the ATO NPs [30].

Fig. 3a shows the XRD curves used to analyze the crystal structure of the films. All the curves exhibit a broad diffraction peak emitted at $\sim 23.1^\circ$, that corresponds to amorphous WO_3 , which potentially has advantageous of EC properties due to fast ion transfer via an open lattice structure [31]. However, no apparent peaks related to ATO NPs were observed in the nanocomposite films due to the very small addition amount of ATO NPs. Therefore, we attempted to characterize the chemical bonding state of the films using X-ray photoelectron spectroscopy (XPS, AXIS ultra-delay line detector equipped with an Al K_α X-ray source, KBSI Daedeok Headquarters). All binding energies were standardized with the C 1s (284.5 eV) as a reference. The W 4f XPS core-level spectra (see Fig. 3b) of all films had one pair of doublets at 35.2 eV for W 4f_{7/2} and 37.3 eV for W 4f_{5/2} which corresponds to the binding energy of W^{6+} . This result is indicative of the successful formation of the WO_3 phase without variation of the chemical bonding state by the addition of different amounts of ATO NPs. However, according to the Sn 3d core-level spectra (see Fig. 3c), noticeable differences in the detected intensity among the samples were observed. Except for the bare WO_3 samples, one pair of doublets at 495.2 eV for Sn 3d_{3/2} and 486.8 eV for Sn 3d_{5/2} was detected in the range of the broad peak of W 4f_{7/2} at 494.3 eV, which corresponds to the binding energy of Sn^{4+} . In the O 1s core-level spectra (see Fig. 3d), it was determined that the magnitude of the peak at 530.8 eV that corresponds to Sb–O bonding gradually increased with an increase in the addition amount of ATO NPs. Based on these results, the formation of the ATO- WO_3 nanocomposite structure was confirmed with an increase in the addition amount of ATO NPs. This can lead to an enhancement of the electrical properties due to the well-dispersed ATO NPs.

To characterize the electrical properties of the nanocomposite films with different addition amount of ATO NPs, the electrical conductivity of the films that were coated onto a bare glass substrate (corning EAGLE XG™) was measured using a Hall-effect measurement system (Ecopia, HMS-3000). Electrical conductivity (see Fig. 4a) is observed to increase from 4.89×10^{-8} S/cm for bare WO_3 to 5.71×10^{-8} S/cm for the 1.2ATO- WO_3 samples. This is due to the decrease in the interparticle distance the of well-dispersed ATO NPs with high electrical conductivity of the WO_3 films. As a result, preferred electron channels develop in these films. However, 2.4ATO- WO_3 samples showed decreased electrical conductivity (5.57×10^{-8} S/cm) due to aggregation by an excessive addition amount of ATO NPs to increase the interparticle distance among the ATO NPs. In addition, the variation of the

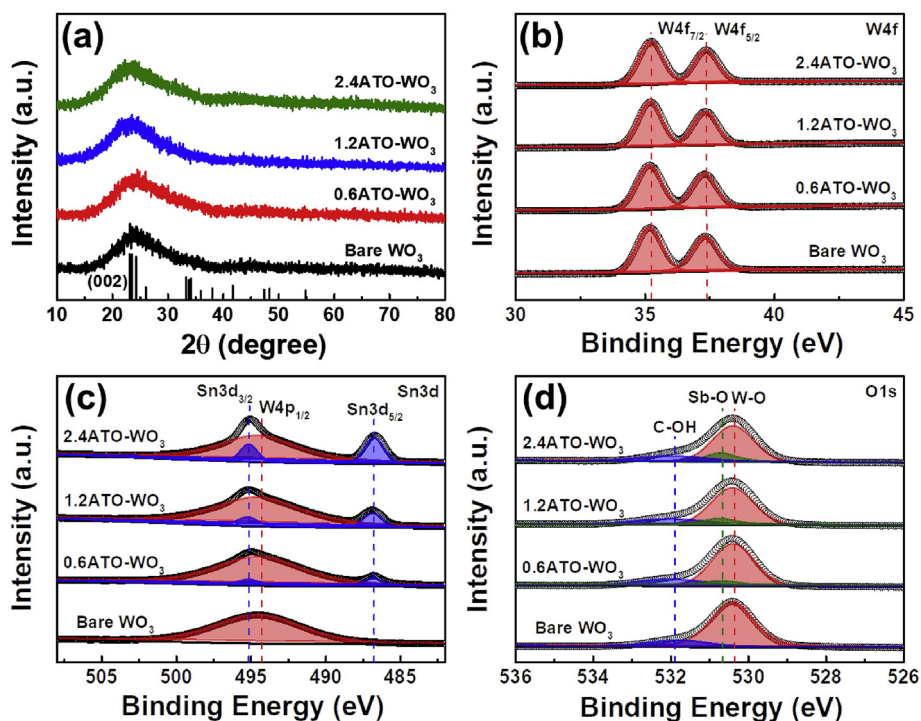


Fig. 3. (a) XRD curves, XPS core-level spectra of (b) W 4f and (c) Sn 3d, and (d) O 1s for all samples.

bandgap of the nanocomposite films with different ATO NPs was investigated using UV–vis spectroscopy (Perkim–Elmer, Lambda–35). Fig. 4b shows the values of the bandgap energy calculated based on fundamental absorption. These results are indicative of electron excitation from the valance band to the conduction band. The correlation between the absorption coefficient (α) and the incident photon energy ($h\nu$) can be written as follows [32,33]:

$$(ah\nu)^{1/n} = A(h\nu - E_g) \quad (2)$$

where A is a constant, E_g is the band gap and n is the type of transition ($n = 1/2$ for allowed direct transitions). The direct bandgap of the films, which was determined by extrapolation of the linear region of the graph between $(ah\nu)^2$ and $h\nu$, were enhanced as the addition amount of ATO NPs increased. The increase in the band gap from the bare- WO_3 (2.75 eV) to the 1.2ATO- WO_3 (2.82 eV) is due to the increased amount of well-dispersed ATO NPs with a large band gap (~ 4.1 eV) compared to WO_3 (~ 2.74 eV) [31]. However, for the 2.4ATO- WO_3 samples, there is a relaxation of the band gap widening due to aggregation of exceeding amount of ATO NPs, leading to a decrease in the band gap [34]. Therefore, the electrical and optical properties of the WO_3 films were successfully modified using ATO- WO_3 nanocomposite structure which can directly affect EC performances.

Cyclic voltammetry (CV) measurement was performed to investigate the effect of the ATO NPs on the electrochemical behavior of the nanocomposite films, which includes electron and ion transfer during the EC reaction. During each CV cycling, all films exhibited reversible color variation from deep blue (colored state) to transparent (bleached state) as a result of the intercalation/deintercalation of Li ions associated with the redox reaction of the WO_3 films (see Eq. (1)). The CV curves of all the films at a scan rate of 20 mV/s are shown in Fig. 5a with one pair of anodic and cathodic peaks. The anodic and cathodic current density were shifted to higher and lower potentials, respectively, gradually increasing from bare WO_3 to 1.2ATO- WO_3 . This result implies that the enhancement of the electrochemical activity is attributed to the increased number of participating ions and electrons during the electrochemical reaction. However, a slight reduction in current density was observed for the 2.4ATO- WO_3 samples which is in good agreement with the electrical conductivity results [35]. In order to evaluate the correlation between them, the diffusion coefficient (D) of the Li ions was determined according to the variation of the current density as the scan rate was changed according to the Randles–Sevcik equation [36,37]:

$$J_p = 2.72 \times 10^5 \times D^{1/2} \times C_o \times \nu^{1/2} \quad (3)$$

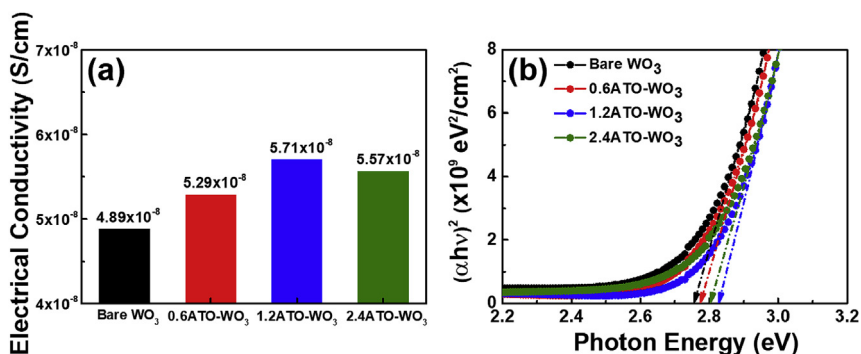


Fig. 4. (a) Electrical conductivity and (b) optical band gap energy of all samples measured in wavelength range from 200 to 800 nm.

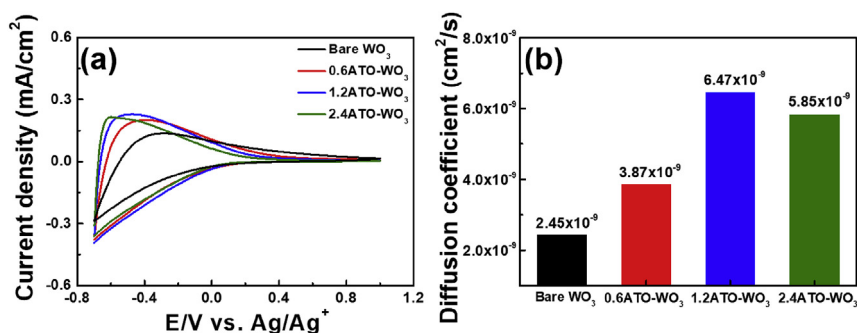


Fig. 5. (a) CV curves of all samples recorded between -0.7 and 1.0 V at the scan rate of 20 mV/s using the three-electrode system and (b) calculated diffusion coefficient of all samples.

where J_p is the peak current density, C_o is the concentration of active ions in the electrolyte, and v is the scan rate for CV profiling. As can be seen in Fig. 5b, the diffusion coefficient of the Li ions increased from 2.45×10^{-9} cm²/s for bare WO₃ to 3.87×10^{-9} cm²/s for 0.6ATO-WO₃ and 6.47×10^{-9} cm²/s for 1.2ATO-WO₃. This result is mainly due to the accelerated reaction rate associated with the improved electrical conductivity because of the effect of the well-dispersed ATO NPs. Given that the redox reaction is associated with electron and ion transportation, enhancement of electron mobility can directly affect the diffusion rate of the Li ions [38]. As such, despite the higher addition amount of ATO NPs, the decreased in the diffusion coefficient (5.85×10^{-9} cm²/s) of the 2.4ATO-WO₃ samples compared to the 1.2ATO-WO₃ samples is due to the reduction of their electrical conductivity due to aggregation of ATO NPs. Therefore, an optimized diffusion coefficient of Li ions and the electrical conductivity of the 1.2ATO-WO₃ samples can improve the EC kinetics which significantly influences EC performance including the switching speeds and CE value [18].

To characterize the EC performances of the samples, the *in situ* optical transmittance at 633 nm was traced to identify the responses during the redox reaction. Fig. 6a shows the curve of the *in situ* optical transmittance of all the measured samples by applying stepped potential of -0.7 V for the colored (deep blue) state and 1.0 V for the bleached (transparent) state for 60 s, respectively. The obtained curves show the two aspects of the EC characteristics including the transmittance modulation (ΔT) (which is defined as the transmittance difference between the bleached state (T_b) and the colored state (T_c) of the EC layer) and switching speed (which is defined as the reaching time to be a 90% of the transmittance modulation from the moment when the voltage is applied). As summarized in Table 2, the value of the transmittance modulation increases from 50.57% for bare WO₃ to 52.40% for 1.2ATO-WO₃. This increase is due to an enhancement of the electrochemical activity and band gap widening of the films as a result of the ATO-WO₃ nanocomposite structure. Therefore, increased electrochemical activity due to the improved electrical conductivity can facilitate the intercalation of Li ions, which reduces transmittance of the

colored state and well-dispersed ATO NPs promote the transmittance of the bleached state. As such, the improved switching speeds are clearly observed as we transition from the bare WO₃ samples (9.7 s for the coloration and 11.1 s for the bleaching speed) to 1.2ATO-WO₃ samples (5.4 s for the coloration and 2.4 s for the bleaching speed). The improvement in switching speeds is attributable to the high conductivity of well-dispersed ATO NPs within the WO₃ films which forms preferred electron channels. However, a large amount of ATO NPs can cause aggregation and a reduction of the switching speeds as observed in the 2.4ATO-WO₃ samples (5.8 s for the coloration and 2.6 s for the bleaching speed). Furthermore, the CE value, which implies that the optical density (OD) variation due to intercalated charge densities (Q/A) is a crucial evaluation factor in determining EC performance. In addition, the CE value was calculated using Eq. (4) [39,40]:

$$CE = \Delta OD / (Q/A) \quad (4)$$

$$\Delta OD = \log (T_b/T_c) \quad (5)$$

where Q is the total quantity of the current for the time period from the bleached to colored state and A is the given electrode area. To achieve a high CE value, the EC layer should exhibit a large OD (related to transmittance modulation) within a small charge density. The CE values obtained by extrapolation of the linear region measured at 633 nm are summarized in Table 2. The CE values were 38.9 cm²/C for bare WO₃, 42.8 cm²/C for 0.6ATO-WO₃, 48.2 cm²/C for 1.2ATO-WO₃ and 43.24 cm²/C for 2.4ATO-WO₃. Therefore, we demonstrated that the optimized CE value (48.2 cm²/C) was mainly due to the high conductivity of ATO-WO₃ nanocomposite structure with well-dispersed ATO NPs.

4. Conclusion

In this study, ATO-WO₃ nanocomposite structure was successfully fabricated on FTO glass using a sol-gel spin-coating method by adjusting the addition amount of ATO NPs (0 , 0.6 , 1.2 , 2.4 wt%). We confirmed the effects of well-dispersed ATO NPs within the amorphous

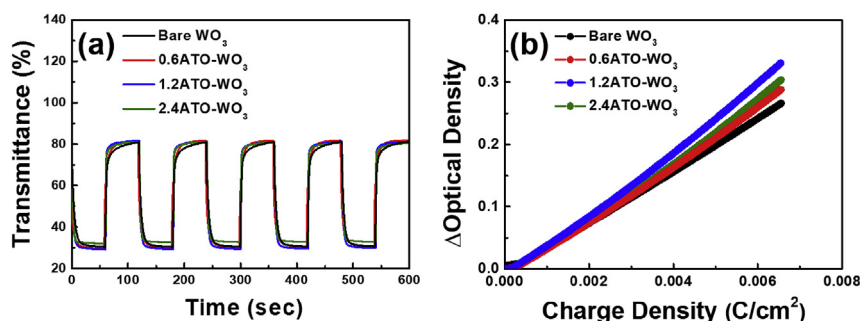


Fig. 6. (a) *In situ* optical transmittance curves of all samples traced in stepping potential at -0.7 V for the colored state and 1.0 V for the bleached state for 60 s and (b) optical density variation at 633 nm with respect to the inserted charge density.

Table 2
Summary of EC performances measured from all samples.

Samples	T _b (%)	T _c (%)	Transmittance modulation (%)	Coloration speed (s)	Bleaching speed (s)	CE (cm ² /C)
Bare WO ₃	80.89	30.31	50.57	9.7	11.1	38.9
0.6ATO-WO ₃	81.06	29.90	51.15	7.0	4.2	42.8
1.2ATO-WO ₃	81.62	29.21	52.40	5.4	2.4	48.2
2.4ATO-WO ₃	81.51	32.77	48.55	5.8	2.6	43.2

WO₃ films which resulted in an enhancement of the electrochemical activity and transmittance modulation. These results suggest that the well-dispersed ATO NPs can effectively improve electrical conductivity and widen the band gap of WO₃ films. As such, the 1.2ATO-WO₃ samples exhibited an optimized nanocomposite effect of ATO NPs and WO₃ films with enhanced EC performances including switching speeds (5.4 s for the coloration speed and 2.4 s for the bleaching speed) and CE value (48.2 cm²/C). This improvement of the EC performances can be attributed to the formation of preferred electron pathways and enhanced band gaps of WO₃ films by well-dispersed ATO NPs. Therefore, we demonstrated the potential of ATO-WO₃ nanocomposite structures in the fabrication of high-performance EC materials. This improvement in EC performances can contribute to further EC research into conductive oxide nanocomposite structures with unique characteristics.

Acknowledgements

This study was supported by the Research Program funded by the SeoulTech (Seoul National University of Science and Technology)

References

- M. Layani, P. Darmawan, W.L. Foo, L. Liu, A. Kamyshny, D. Mandler, S. Magdassi, P.S. Lee, Nanostructured electrochromic films by inkjet printing on large area and flexible transparent silver electrodes, *Nanoscale* 6 (2014) 4572–4576.
- H. Li, G. Shi, H. Wang, Q. Zhang, Y. Li, Self-seeded growth of nest-like hydrated tungsten trioxide film directly on FTO substrate for highly enhanced electrochromic performance, *J. Mater. Chem.* 2 (2014) 11305–11310.
- G. Cai, P. Darmawan, M. Cui, J. Chen, X. Wang, A.L.-S. Eh, S. Magdassi, P.S. Lee, Inkjet-printed all solid-state electrochromic devices based on NiO/WO₃ nanoparticle complementary electrodes, *Nanoscale* 8 (2016) 348–357.
- S.K. Deb, A novel electrophotographic system, *Appl. Opt.* 8 (1969) 192–195.
- R.-T. Wen, C.G. Granqvist, G.A. Niklasson, Eliminating degradation and uncovering ion-trapping dynamics in electrochromic WO₃ thin films, *Nat. Mater.* 14 (2015) 996–1001.
- P. Simon, Y. Gogotsi, Materials for electrochemical capacitors, *Nat. Mater.* 7 (2008) 845–854.
- B. Jiang, B. Luo, J. Li, P. Peng, J. Chen, L. Chu, Y. Li, M. Li, Electrochemical effect of graphite fluoride modification on Li-rich cathode material in lithium ion battery, *Ceram. Int.* 45 (2019) 160–167.
- B.-R. Koo, H.-J. Ahn, Fast-switching electrochromic properties of mesoporous WO₃ films with oxygen vacancy defects, *Nanoscale* 9 (2017) 17788–17793.
- G. Cai, J. Wang, P.S. Lee, Next-generation multifunctional electrochromic devices, *Acc. Chem. Res.* 49 (2016) 1469–1476.
- K.R. Reyes-Gil, Z.D. Stephens, V. Stavila, D.B. Robinson, Composite WO₃/TiO₂ nanostructures for high electrochromic activity, *ACS Appl. Mater. Interfaces* 7 (2015) 2202–2213.
- L. Zhu, C.K.N. Peh, T. Zhu, Y.-F. Lim, G.W. Ho, Bifunctional 2D-on-2D MoO₃ nanobelt/Ni(OH)₂ nanosheets for supercapacitor-driven electrochromic energy storage, *J. Mater. Chem.* 5 (2017) 8343–8351.
- C.G. Granqvist, Electrochromics for smart windows: oxide-based thin films and devices, *Thin Solid Films* 564 (2014) 1–38.
- G.A. Niklasson, C.G. Granqvist, Electrochromics for smart windows: thin films of tungsten oxide and nickel oxide, and devices based on these, *J. Mater. Chem.* 17 (2007) 127–156.
- C.G. Granqvist, Electrochromic materials: out of a niche, *Nat. Mater.* 5 (2006) 89–90.
- X. Liu, A. Zhou, Y. Dou, T. Pan, M. Shao, J. Han, M. Wei, Ultrafast switching of an electrochromic device based on layered double hydroxide/Prussian blue multilayered films, *Nanoscale* 7 (2015) 17088–17095.
- K.-H. Kim, B.-R. Koo, H.-J. Ahn, Sheet resistance dependence of fluorine-doped tin oxide films for high-performance electrochromic devices, *Ceram. Int.* 44 (2018) 9408–9413.
- J.-W. Bae, B.-R. Koo, H.-J. Ahn, Fe doping effect of vanadium oxide films for enhanced switching electrochromic performances, *Ceram. Int.* 45 (2019) 7137–7142.
- F. Zheng, W. Man, M. Guo, M. Zhang, Z. Qiang, Effects of morphology, size and crystallinity on the electrochromic properties of nanostructured WO₃ films, *Crystengcomm* 17 (2015) 5440–5450.
- S. Heo, J. Kim, G.K. Ong, D.J. Milliron, Template-free mesoporous electrochromic films on flexible substrates from tungsten oxide nanorods, *Nano Lett.* 17 (2017) 5756–5761.
- J.Z. Ou, S. Balendhran, M.R. Field, D.G. McCulloch, A.S. Zoolfakar, R.A. Rani, S. Zhuiykov, A.P. O'Mullane, K. Kalantar-zadeh, The anodized crystalline WO₃ nanoporous network with enhanced electrochromic properties, *Nanoscale* 4 (2012) 5980–5988.
- S.R. Bathe, P.S. Patil, Electrochromic characteristics of fibrous reticulated WO₃ thin films prepared by pulsed spray pyrolysis technique, *Sol. Energy Mater. Sol. Cells* 91 (2007) 1097–1101.
- X. Yang, G. Zhu, S. Wang, R. Zhang, L. Lin, W. Wu, Z.L. Wang, A self-powered electrochromic device driven by a nanogenerator, *Energy Environ. Sci.* 5 (2012) 9462–9466.
- K. Gesheva, A. Szekeles, T. Ivanova, Optical properties of chemical vapor deposited thin films of molybdenum and tungsten based metal oxides, *Sol. Energy Mater. Sol. Cells* 76 (2003) 563–576.
- M. Deepa, T.K. Saxena, D.P. Singh, K.N. Sood, S.A. Agnihotry, Spin coated versus dip coated electrochromic tungsten oxide films: structure, morphology, optical and electrochemical properties, *Electrochim. Acta* 51 (2006) 1974–1989.
- J. Han, K.-W. Ko, S. Sarwar, M.-S. Lee, S. Park, S. Hong, C.-H. Han, Enhanced electrochromic properties of TiO₂ nanocrystal embedded amorphous WO₃ films, *Electrochim. Acta* 278 (2018) 396–404.
- J. Kim, G.K. Ong, Y. Wang, G. Leblanc, T.E. Williams, T.M. Mattox, B.A. Helms, D.J. Milliron, Nanocomposite architecture for rapid, spectrally-selective electrochromic modulation of solar transmittance, *Nano Lett.* 15 (2015) 5574–5579.
- J.M. Bolts, M.S. Wrighton, Correlation of photocurrent-voltage curves with flat-band potential for stable photoelectrodes for the photoelectrolysis of Water, *J. Phys. Chem.* 80 (1976) 2641–2645.
- L. Ding, S. He, S. Miao, M.R. Jorgensen, S. Leubner, C. Yan, S.G. Hickey, A. Eychmüller, J. Xu, O.G. Schmid, Ultrasmall SnO₂ nanocrystals: hot-bubbling synthesis, encapsulation in carbon layers and applications in high capacity Li-ion storage, *Sci. Rep.* 4 (2014) 4647.
- Y. Li, J. Wang, B. Feng, K. Duan, J. Weng, Synthesis and characterization of antimony-doped tin oxide (ATO) nanoparticles with high conductivity using a facile ammonia-diffusion co-precipitation method, *J. Alloy. Compd* 634 (2015) 37–42.
- W. Posthumus, J. Laven, G.D. With, R.V.D. Linde, Control of the electrical conductivity of composites of antimony doped tin oxide (ATO) nanoparticles and acrylate by grafting of 3-methacryloxypropyltrimethoxysilane (MPS), *J. Colloid Interface Sci.* 304 (2006) 394–401.
- L. Xiao, Y. Lv, W. Dong, N. Zhang, X. Liu, Dual-functional WO₃ nanocolumns with broadband antireflective and high-performance flexible electrochromic properties, *ACS Appl. Mater. Interfaces* 8 (2016) 27107–27114.
- S. Shanthi, C. Subramanian, P. Ramasamy, Investigations on the optical properties of undoped, fluorine doped and antimony doped tin oxide films, *Cryst. Res. Technol.* 8 (1999) 1037–1046.
- B.-R. Koo, K.-H. Kim, H.-J. Ahn, Switching electrochromic performance improvement enabled by highly developed mesopores and oxygen vacancy defects of Fe-doped WO₃ films, *Appl. Surf. Sci.* 453 (2018) 238–244.
- M.J. O'connell, S.M. Bachilo, C.B. Huffman, V.C. Moore, M.S. Strano, E.H. Haroz, K.L. Rialon, P.J. Boul, W.H. Noon, C. Kittrell, J. Ma, R.H. Hauge, R.B. Weisman, R.E. Smalley, Band gap fluorescence from individual single-walled carbon nanotubes, *Science* 297 (2002) 593–596.
- J. Xu, Z. Liao, J. Zhang, B. Gao, P.K. Chu, K. Huo, Heterogeneous phosphorus-doped WO_{3-x}/nitrogen-doped carbon nanowires with high rate and long life for advanced lithium-ion capacitors, *J. Mater. Chem.* 6 (2018) 6916–6921.
- H. Kim, D. Choi, K. Kim, W. Chu, D.-M. Chun, C.S. Lee, Effect of particle size and amorphous phase on the electrochromic properties of kinetically deposited WO₃ films, *Sol. Energy Mater. Sol. Cells* 177 (2018) 44–50.
- B.-R. Koo, K.-H. Kim, H.-J. Ahn, Novel tunneled phosphorus-doped WO₃ films achieved using ignited red phosphorus for stable and fast switching electrochromic performances, *Nanoscale* 11 (2019) 3318–3325.
- G. Yuan, C. Hua, S. Khan, S. Jiang, Z. Wu, Y. Liu, J. Wang, C. Song, G. Han, Improved electrochromic performance of WO₃ films with size controlled nanorods, *Electrochim. Acta* 260 (2018) 274–280.
- A. Zhou, X. Liu, Y. Dou, S. Guan, J. Han, M. Wei, The fabrication of oriented organic-inorganic ultrathin films with enhanced electrochromic properties, *J. Mater. Chem. C* 4 (2016) 8284–8290.
- G. Cai, M. Cui, V. Kumar, P. Darmawan, J. Wang, X. Wang, A.L.-S. Eh, K. Qian, P.S. Lee, Ultra-large optical modulation of electrochromic porous WO₃ film and the local monitoring of redox activity, *Chem. Sci.* 7 (2016) 1373–1382.